Rare coding variants in CTSO , a potential new actor of arterial remodeling, are associated to familial intracranial aneurysm

Milène Fréneau, Raphaël Blanchet, Sandro Benichi, Mary-Adel Mrad, Surya Prakash Rao Batta, Marc Rio, Stéphanie Bonnaud, Pierre Lindenbaum, Fabien Laporte, Stéphane Cuenot, et al.

Rare coding variants in *CTSO*, a potential new actor of arterial remodeling, are associated to familial intracranial aneurysm

Milène Freneau[1,5], Raphael Blanchet[1,5], Sandro Benichi[1], Mary-Adel Mrad[1], Surya Prakash Rao Batta[1], Marc Rio[1], Stéphanie Bonnaud[1], Pierre Lindenbaum[1], Fabien Laporte[1], Stéphane Cuénot[2], Jean-François Deleuze[3], Christian Dina[1], Stéphanie Chatel[1], Emmanuelle Bourcereau[4], Solène Jouan[4], ICAN Study Group, Hubert Desal[1,4], Anne-Clémence Vion[1], Romain Bourcier[1,4,5], Gervaise Loirand[1,5], Richard Redon[1,5].

[1] Nantes Université, CHU Nantes, CNRS, INSERM, l'institut du thorax, F-44000 Nantes, France

[2] Nantes Université, CNRS, Institut des Matériaux Jean Rouxel, IMN, F-44000 Nantes, France

[3] Université Paris-Saclay, CEA, Centre National de Recherche en Génomique Humaine (CNRGH), F-91057 Evry, France

[4] Department of Neuroradiology, CHU Nantes, F-44000 Nantes, France

[5] These authors contributed equally to this work as first and last authors

*Correspondence: Gervaise Loirand (gervaise.loirand@univ-nantes.fr) & Richard Redon (richard.redon@univ-nantes.fr)

Running title: *CTSO* and intracranial aneurysm

Key words: Genetics, intracranial aneurysm, cathepsin, cerebral artery, smooth muscle, extracellular matrix, fibronectin, stiffness

Abstract

Background: Intracranial aneurysm (IA) is a common cerebrovascular abnormality characterized by localized dilation and wall thinning in intracranial arteries, that frequently leads to fatal vascular rupture. The mechanisms underlying IA formation, growth and rupture are mostly unknown, and while increasing evidence suggest a genetic component of IA, identification of specific genes or causal molecular pathways remains largely inconclusive and only a small fraction of the risk attributable to genetics for IA in the general population.

Methods: Here, we combined whole exome sequencing and identity-by -descent analyses with functional investigations to identify rare IA predisposing variants in familial forms of IA and understand their contribution to the pathophysiology of IA.

Results: We identified two rare missense variants in the *CTSO* gene shared by all the affected relatives in two large pedigrees with multiple IA-affected relative. *CTSO* encodes for the cysteine-type papain-like cathepsin CTSO. Functional analyses revealed that CTSO acts as an extracellular protease controlling vascular smooth muscle cell migration and adhesion to the extracellular matrix. CTSO depletion, as well as expression of the two CTSO variants, which were poorly secreted, led to increase the amount of fibronectin. This effect is associated with a marked increase in VSMC stiffness which was rescued by exogenous CTSO.

Conclusions: This report identifies rare CTSO variants in familial IA patients and suggests that the increased susceptibility to IA induced by these variants is likely related to their primary effects on the vascular tissue, and more particularly on the media layer of the wall of cerebral arteries.

Introduction

Intracranial aneurysm (IA) is a generally asymptomatic localized dilation associated with thinning and structural defects of intracranial arterial wall affecting 1-5% of the general population.[1] The devastating complication of IA is its unpredictable rupture, responsible for ~36,000 cases of subarachnoid hemorrhage in Europe and a major cause of sudden death in "young healthy" subjects, in particular in woman (peak of age: 50-60 years).[2, 3] Although hypertension, ageing, female gender, smoking, excessive alcohol consumption and family history of IA have been identified as risk factors predisposing to IA, the mechanisms underlying IA formation, growth and rupture are mostly unknown, although the local hemodynamic constraints of shear stress and pressure are assumed to play a key role.[4] The aggregation of patients in IA families suggests that genetic factors contribute to disease susceptibility, and identifying these factors might be beneficial for at-risk patients before IA rupture.[5, 6] Genome-wide association studies have identified several common risk loci associated with IA.[7-10] However, identification of specific genes or causal molecular pathways remains largely inconclusive and these common alleles together explain only a small fraction of the risk attributable to genetics for IA in the general population. On the other hand, whole-exome sequencing (WES) has the potential to detect rare coding variants that have large effect and induce a high risk of developing IA. Identifying such variants also could provide valuable insights into the pathophysiology of IA and pave the way for new diagnostic or therapeutic strategies. Indeed, recent studies have demonstrated the usefulness of familial approaches based on WES to improve knowledge on the molecular mechanisms underlying IA formation and rupture from the discovery of rare predisposing variants such as *RNF213*,[11] *THSD1*,[12] *LOXL2*,[13] *PCNT*,[14] *ARHGEF17*, [15] *ANGPTL6,*[16] and *PPIL4*.[17]

In the present study, by combining WES and identity-by-descent (IBD) analysis, we identified rare coding variants in the Cathepsin O gene (*CTSO* [MIM: 600550]) as causally related to

familial forms of IA. CTSO is one of the 11 cysteine-type papain-like cathepsins identified in human about almost nothing is known.[18] Functional analysis revealed that CTSO controls vascular smooth muscle cell (VSMC) migration and adhesion to the extracellular matrix (ECM). Furthermore, CTSO depletion leads to increase VSMC stiffness. These finding suggest that the increased susceptibility to IA induced by *CTSO* variants is likely related to their primary effects on the vascular tissue, and more particularly on the media layer of the wall of cerebral arteries.

Results

Identification of one rare coding variant affecting *CTSO* in a familial case of IA

We first recruited a large family (Figure 1A) with 6 definite carriers of IA in two generations, among whom two had a history of IA rupture. In this family, there were also 4 relatives with suspected IA (3 because of unexplained sudden death and 1 with a doubtful ectasia on MRI (III-14)), 4 individuals with unknown phenotypes that have not been screened by MRI and 19 subjects without IA detected on MRI. Among the definite carriers of IA, all were females and 3 were carriers of multiples IA. The median maximal diameter of IA was 4 mm (min 3 mm, max 8 mm). Of the twelve IAs detected in the family, 6 were located in the MCA territory (50%), 3 in the ACA (25%), 2 in the PCA (16%), and 1 in the ICA territory (9%). We applied whole-exome sequencing to 3 affected members of the family (II9, III2, III4; Figure 1A). Out of the 153 to 179 rare non-synonymous or splicing variants detected in each 3 whole exomes, we found that only 16 were shared between the 3 affected relatives (Table 1). We then performed IBD analysis of the complete pedigree to test whether each variant resides within one haplotype shared by the 6 affected relatives. We found that only one of the 16 variants is located in one shared haplotype at 4q32, then confirmed by capillary sequencing its presence for all affected relatives. This missense variant in the *CTSO* gene - *CTSO* c.946G>A

(p.Val316Ile) - is reported with a Genomic Evolutionary Rate Profiling (GERP) score of 5.68 and predicted as damaging *in silico* by both PolyPhen-2 and SIFT (Table 2).

A second familial case of IA associated with rare coding variant in *CTSO*

To further investigate the putative involvement of *CTSO* in IA susceptibility, we then screened for rare coding variants within this gene among 93 additional index cases with familial forms of IA (with at least two affected first-degree relatives), for which WES data were available in-house. We found one rare missense variant, *CTSO* c.128C>T (p.Ala43Val) (Table 1). The corresponding family (Figure 1B) comprises 5 IA carriers (3 females and 2 males), among whom one carries multiple IAs. The median maximal diameter of IA was 5 mm (min 4 mm, max 9 mm). Three IAs are located in the MCA territory, one in the ACA and one in the ICA territory, while one is of unknown located. By capillary sequencing, we tested the *CTSO* c.128C>T variant among family members and detected it in the 3 tested IA carriers but in none of their 5 unaffected relatives (with available DNA). This variant, reported with a GERP score of 3.67, is predicted as damaging *in silico* by PolyPhen-2 but not by SIFT (Table 2).

Clinical characteristics and exposition to risk factors according to *CTSO* status

When comparing subgroups of individuals without or with *CTSO* variant and carrying or not IA among the members of the two families, we observed a higher proportion of subjects with history of high blood pressure among the IA carriers ($p<0.01$) while we found no significant differences regarding age, proportion of women, smoking habits, history of ischaemic stroke, level of alcohol consumption, history of diabetes or dyslipidaemia, treatment with statin, antiplatelet, oral anticoagulant and anti-inflammatory medication (Table 3).

CTSO is expressed in cerebral arteries

To explore the putative implication of CTSO in IA pathophysiology, we first sought to investigate the expression of CTSO in cerebral arteries. *Ctso* mRNA was indeed found in cerebral arteries of WKY rats, and at a similar level, in artery from spontaneously hypertensive rat (SHR) and stroke prone SHR (SPSHR), suggesting that *Ctso* mRNA expression was not modulated by high blood pressure (Figure 2A). At cell level, *Ctso* mRNA was expressed in VSMC and, at weaker levels, in endothelial cells, where it was not modulated by shear stress (SS) (Figure 2B, Figure S1). In smooth muscle cell cultures, CTSO was found in cell lysates but also in the culture medium, indicating the secretion of the protein (Figure 2C). Moreover, CTSO secretion was potentiated by stretch, without any change in mRNA level (Figure 2B and C).

***Ctso* silencing does not affect VSMC proliferation and apoptosis**

We next aimed to elucidate the role of CTSO in the arterial wall by focusing on VSMC in which it is predominantly expressed and modulated by stretch. To this end, we evaluated the consequences of siRNA-mediated depletion of endogenous CTSO in vascular smooth muscle cells (KD-SMC) in comparison with a control siRNA pool. Silencing of *Ctso* did not affect VSMC proliferation (Figure 2D), nor apoptosis as measured by TUNEL and caspase 3 cleavage in basal condition (no apoptosis, data not shown) and after induction of apoptosis by staurosporine (Figure 2E and F). These results indicate that CTSO did not affect VSMC proliferation and viability.

***Ctso* silencing modifies VSMC migration and adhesion**

We next tested whether CTSO regulates the migratory and adhesive properties of VSMC by using Boyden chambers and adhesion assays, respectively. CTSO depletion in VSMC (KD-

SMC) led to a significant decrease in transmigration (Figure 3A) but accelerated the adhesion speed of VSMC on fibronectin (FN) matrix (Figure 3B). This effect was associated with an increased phosphorylation of focal adhesion kinase (FAK) in KD-SMC compared to control SMC (Cont-SMC), both at 2 h and 24 h after seeding on FN matrix (Figure 3C). When VSMC were plated on plastic, without FN coating, a significant increase in FAK phosphorylation was also observed at 24 h but not at 2 h post-seeding (Figure 3D). It is known that SMC produced and released FN which, in turn, can modulate VSMC phenotype and functions.[19] The observed differences in FAK phosphorylation induced by CTSO depletion may results from an effect on the endogenous FN. To test this hypothesis, we thus analyzed the effect of *Ctso* silencing on FN expression in Cont- and KD-SMC culture. An increased level of FN was observed in KD-SMC compared to Cont-SMC, while there was no difference in the Collagen I (COL-I) expression (Figure 3E). This rise in FN expression was not associated with a change in mRNA-Fn1 level which, like mRNA-*Col1a* expression, remains the same in Cont- and KD-SMC (Figure 4A). All together, these data show that CTSO controls VSMC migration and adhesion, and suggest that it could result from an effect on the amount of FN released by SMC.

Ctso silencing affects contractile phenotype marker gene expression

We next assessed the potential role of CTSO on VSMC phenotype by measuring the expression of contractile marker gene expression (Figure 4B). The expression of all tested VSMC marker genes, namely *Acta2, Myh11*, *Tagln* and *Cnn1* were significantly up-regulated by *Ctso* silencing, which was also checked (Figure 4C). By contrast, the expression of *Bmp4*, a known marker of osteogenic differentiation of VSCM[20] differentiation was reduced in KD-SMC compared to Cont-SMC (Figure 4C). These results suggest that *Ctso* silencing positively modulated VSMC differentiation. However, measurement of contractility showed

that KD-SMC contracted collagen gel less strongly than Cont-SMC in response to the thromboxane A2 analog U46619 (Figure 4D).

Ctso silencing induces stiffening of VSMC

We then used atomic force microscopy (AFM) to assess the effect of CTSO depletion on the stiffness of VSMC and VSCM-derived extracellular matrix (ECM) as arterial stiffening is known to be a risk factor for IA.[21] Elastic modulus determined by AFM nanoindentation showed that KD-SMC were significantly stiffer than Cont-SMC, while the corresponding ECM produced by KD- and Cont-SMC displayed a similar stiffness (Figure 4E and S2).

CTSO variants

To assess the impact of c.128C>T *CTSO* and c.946G>A *CTSO* variants on CTSO protein we established stable cell lines expressing the wild-type (WT-CSTO), and the two mutated proteins, p.Val316Ile-CTSO and p.Ala43Val-CTSO. Western blot analysis shows that expression level in cell lysates was similar for WT-CTSO and the two mutated proteins (Figure 5A). In contrast, the amount of p.Val316Ile-CTSO and p.Ala43Val-CTSO in the culture medium was strongly reduced compared to WT-CTSO (Figure 5A). Since we observed an increase in the amount of FN after CTSO depletion in VSMC (Figure 3E), we investigated the effect of p.Val316Ile-CTSO and p.Ala43Val-CTSO expression on FN level. Western-blot results show that CTSO mutants mimicked the effect of CTSO depletion on the increase of FN level, without effect on COL-I expression (Figure 5B).

Discussion

We have identified two rare missense variants in the *CTSO* gene shared by all the affected relatives in two large pedigrees with multiple IA-affected relative. Of note, we observed a few

individuals (n=6) carrying possibly deleterious *CTSO* variations but without IA at the time of the study. In addition, we found a significant increase in the proportion of subjects with history of high blood pressure among IA careers compared to unaffected individuals. High blood pressure history is a well-established environmental factor associated with the development of IA.[22] Our results suggest, as described previously in familial cases with rare coding variants in *ANGPTL6*,[16] that rare coding variants in *CTSO* could thus promote IA formation in combination with other deleterious genetic or environmental factors such as high blood pressure, which would act either directly by mechanical effects on the vessel walls or indirectly by triggering inflammation.[23]

CTSO is one of the 11 cathepsins encoded in the human genome which constitute an important group of proteases that regulate numerous processes.[18] They are highly expressed in intracellular acidic compartments such as endosomes and lysosomes, and loss of function mutations in cathepsin genes cause very different syndromes in terms of clinical symptoms and disease progression, corresponding to either typical lysosomal storage diseases, or resulting from defective cleavage of specific protein substrates.[24] Cathepsins are also found in the cytoplasm, cell nucleus, cell membrane and the extracellular space.[25, 26] Extracellular cathepsins mediate extracellular matrix (ECM) protein degradation (collagen, elastin, fibronectin, laminin) and release of ECM-bound factors, but also shed various membrane proteins including receptors, growth factors, cytokines, and adhesion proteins thereby influencing important cellular processes such as proliferation and differentiation, motility, cell-cell interaction, adhesion, inflammatory and immune responses. Indeed, extracellular cathepsins are majorly upregulated in pathological states and are implicated in a wide range of disorders including vascular remodeling and atherosclerotic diseases.[27, 28] Cathepsin B, K and S have been found to be upregulated in the wall of IA.[29] CTSO is defined as a ubiquitous protein but neither its peptidase behavior nor its functions have been characterized. We

observed CTSO expression in cerebral artery wall, endothelial cells, and more strongly in VSMC. In these cells, CTSO was found both in intra- and extracellular compartments, and its extracellular release, probably through lysosomal exocytosis, is stimulated by cell stretching, suggesting that its role as an extracellular protease in the arterial wall could be potentiated by high blood pressure and participated to the arterial remodeling induced by hypertension.

Although we did not analyze the enzymatic activity of CTSO in vitro to directly demonstrate its ability to degrade FN, there is a strong body of experimental evidence to support this hypothesis. Adhesion and FAK activation are potentiated by depletion of CTSO, both rapidly and late after VSMC seeding on exogenous FN coating, while only delayed stimulation of FAK activation was observed in CTSO-depleted VSMC seeded on plastic. These observations are consistent with a degradation of pericellular FN by CTSO, which instantaneously impaired cell-FN coating interaction in VSMC producing extracelullar CTSO. When VSCM are seeded on plastic, the effect of CTSO depletion is only visible late, after the time necessary for the cells to self-produce surrounding FN with which they establish adhesions. This hypothesis is supported by the increase in the amount of FN induced by the depletion of CTSO in VSMC and suggests that extracellular CTSO secreted by VSCM degrades FN.

This was corroborated by the results obtained by the expression of the two mutated proteins p.Val316Ile-CTSO and p.Ala43Val-CTSO which, being weakly secreted, induce an increase in the amount of FN as does the depletion of CTSO.

It is well established that adhesive properties to ECM drives VSMC stiffness,[30] and the level of activation of FAK signaling is related to VSMC stiffness.[31] In particular, VSMC focal adhesion to FN correlated with VSMC stiffness.[32] The strong stiffening of VSMCs that we observed after CTSO depletion is therefore consistent with an increase in the ability of VSMCs to form adhesions to FN due to the reduced degradation of FN in CTSO-depleted VSMCs.

ECM composition and organization impact the physical interactions with VSMC, which play a major role in regulating their functions including, migration and differentiation. We observed that knocking-down CTSO reduced VSMC migration on FN. This result further supports a role of CTSO in promoting FN degradation, although additional mechanisms such as degradation of other extracellular proteins or lysosomal degradation of FN-bound integrins known to be required for migration,[33] could also been involved. Regarding VSMC differentiation, CSTO depletion led to increase the expression of contractile phenotype marker genes such as *Acta2*. Interestingly, deletion or inhibition of cathepsin B, characterized as a FN-degrading protease[34] which was also up-regulated by cell stretching, also increases ACTA2 expression through mechanisms that have not been identified.[35] Increased ACTA2 expression has been shown to contribute to VSMC stiffening,[36] suggesting that up-regulation of *Acta2* and possibly of the other contractile markers, could participate to the increase in VSMC stiffness induced by CTSO depletion. Although contractile markers were upregulated, collagen gel contraction induced by KD-VSMC was reduced compared to Cont-VSMC. Whether this effect was related to the stiffness of VSMCs induced by the CTSO deletion cannot be determined, however, VSMCs from old animals show a similar association of increased stiffness[30] and reduced collagen gel contraction.[32, 37]

Besides their contractile activity, VSMCs normally produce ECM that allows adaptations to mechanical forces that act on the vessel wall while maintaining adequate wall pressures. Thus, the composition, the organization and the resulting interactions of ECM with VSMC is adjusted to the mechanical demands of the vessel wall thanks to multiple and coordinated mechanisms. Among them, the fine-tuning of the expression and activity of extracellular proteases plays a major role in reshaping the ECM matrix. In this study, we identified CTSO as a potential new actor of arterial remodeling that regulates FN deposition and VSMC functions. This role of CTSO is consistent with an increased susceptibility to IA associated

with c.128C>T *CTSO* and c.946G>A *CTSO* variants. We suggest that by promoting increase in FN deposition, VSMC-FN adhesion and VSMC stiffening, p.Val316Ile-CTSO and p.Ala43Val-CTSO mutants affect the mechanical properties of the vessel wall that compromise proper adaptation of the arterial wall to local hemodynamics thereby favoring IA formation. It is noteworthy that similar features, namely faster adhesion to FN,[38] up-regulation of contractile marker expression and increased stiffness have been described in Marfan syndrome VSMC,[39] a well-known genetic condition that predisposes to IA.[40]

Methods

Clinical recruitment

Familial cases of IA are defined as at least two first-degree relatives both diagnosed with typical IA (defined as a saccular arterial dilatation of any size occurring at a bifurcation of the intracranial vasculature), without any age limitation. Index case subjects and their relatives were recruited following the French ethical guidelines for genetic research and under approval from the French Ministry of Research (no. DC-2011-1399) and the local ethical committee. Informed written consent was obtained from each individual agreeing to participate in the genetic study, to whom MRI screening and blood sampling were proposed. The full recruiting process has been described previously.[41] Briefly, neuroradiological phenotyping was performed in each recruiting center by interventional neuroradiologists, neurologists, and neurosurgeons in order to recruit only case subjects with typical saccular bifurcation IA. Mycotic, fusiform-shaped, or dissecting IAs were systematically excluded, as well as IA in relation with an arteriovenous malformation and IA resulting from syndromic disorders such as Marfan disease or vascular forms of Elhers Danlos. For all included patients we recorded the date of birth, if IA, the cases of rupture, the number of IA, the IA larger diameter in mm, the IA locations according to the four following groups internal carotid artery (ICA), posterior cerebral circulation (PCA), Middle cerebral artery (MCA) or anterior cerebral artery (ACA), the smoking habits, the history of high blood pressure and ischemic stroke, the level of alcohol intake per week, the history of diabetes or dyslipidemia, obesity (BMI >30), treatment by statin, antiplatelet, oral anticoagulant and anti-inflammatory drugs.

Whole Exome Sequencing (WES)

Genomic DNA was extracted from peripheral blood lymphocytes using the NucleoSpin Blood kit XL (Macherey Nagel). Whole-exome fragments were captured with to the SureSelect

Human All Exon V4 kit (Agilent technology), according to manufacturer protocol. Alignment on reference genome (Broad Institute human_g1k_v37) was performed using Burrow-Wheeler aligner (Bwa mem v0.7.10).[42] Picard v1.119 was used to flag duplicates and recalibration was achieved through GATK v3.2.2 (broadinstitute, 2023).[43] Variants were called with GATK HaplotypeCaller on all exons hg9 exons (NCBI RefSeq), annotated with SnpEff and vcfGnomad (jvarkit) using gnomad v2.1.[44] Quality filters detailed in the Table S1 were applied. Only variants annotated as non-synonymous or affecting splicing, and reported with a minor allelic frequency (MAF) below 0.1% in the non-Finnish European (NFE) gnomAD population, were subsequently considered.

IBD analysis

Haplotype sharing between affected relatives were identified through IBD analysis basedon SNP genotyping data. Fluorescence intensities were obtained from Precision Medicine Research Array (PMRA - Affymetrix) and quantified by Affymetrix GeneTitan Multi-Channel Instrument. Genotypes were merged with PREGO control population[45] and SNPs with MAF<10%, call rate < 95% or p<1.10-5 when testing for Hardy-Weinberg equilibrium were excluded. IBD regions were then identified using IBDLD v3.34 with noLD method.[46] Familial segregation analysis by capillary sequencing was performed on an Applied Biosystems 3730 DNA Analyzer, using standard procedures. Sequence analyses were performed with SeqScape v.2.5.

Animal model

All animal care and use procedures of the present study were performed in accordance with the European Community Standards on the Care and Use of Laboratory Animals and were

approved by our institutional ethics committee (authorization D44278). Cerebral arteries from 3 months-old Wistar-Kyoto (WKY), spontaneously hypertensive (SHR) and stroke-prone SHR (SPSHR) rats (300 g) were collected and snap-frozen in liquid nitrogen for RNA extraction.

Cell culture

Primary VSMC were isolated from the aorta of 4-week-old WYK rats. Rats were sacrificed according to institutional animal handling ethics. The aorta was harvested, cleaned, endothelium-denuded, cut into small pieces and digested by collagenase II (1 mg/mL; 2 h at 37°C under agitation; Worthington Bio-chemical). After inactivation of collagenase with serum, the tissue was spun down and plated in a 6-well plate in Dulbecco modified Eagle medium (DMEM, Gibco; Invitrogen) containing 10% foetal bovine serum (FBS), 4.5 g/L glucose, 100 units/mL penicillin and 100 µg/mL streptomycin at 37°C-5% CO2. All experiments were performed at passages 2 and 3. For cell stretching, cyclic uniaxial strain was applied at 1 Hz and 10% or 20% strain for 24 hours (MechanoCulture FX, CellScale). HUVEC (passage 2 to 6; PromoCell) were routinely cultured in EBM media supplemented with the provided growth factors kit (Promocell). For flow experiments HUVEC were cultured on 0.2% gelatin-coated 0.4 ibidi slides (IBIDI) and unidirectional laminar shear stress was applied using the pumping system and control unit form IBIDI. Local shear stress was calculated using Poiseuille's law and averaged to 3 dyn/cm^2 (pathological low shear stress: LSS) 16 dyn/cm^2 (physiological shear stress: PSS) or 36 dyn/cm^2 (pathological high shear stress: HSS). NIH3T3 cells were cultured in DMEM containing 1 g/L glucose, 10% FBS, 100 units/mL penicillin and 100 µg/mL streptomycin at 37°C-5% CO2.

RT-PCR

Total RNA was purified from cells using RNA plus kit (Macherey Nagel) or tissue using TRIzol reagent (MAN0001271, Ambion, Thermo Fisher Scientific) and RNA XS Plus kit (Macherey Nagel) according to the manufacturer instructions. RNA (500 ng) was reverse-transcribed with M-MLV enzyme (28025021, Thermo Fisher Scientific). Real-time qPCR was performed on a 7900HT Fast Real-Time PCR System (Applied Biosystems) using SYBR Green Master Mix (4367659, Applied Biosystems) and primers listed in Table S2. Each sample was analyzed in triplicate. GAPDH was used as the reference gene and results are expressed according to the $2^{-\Delta\Delta Ct}$ method.

Immunoblotting

Supernatant from VSMC or NIH3T3 were taken off and concentrated with Amicon Ultra-0.5 Centrifugal Filter Unit (UFC5010, Millipore). Cells were lysed on ice in buffer supplemented with protease and phosphatase inhibitor cocktails (Sigma Aldrich) and sodium orthovanadate. Equal amount of proteins of each sample was separated by SDS-PAGE, transferred to nitrocellulose membranes, and incubated with specific antibodies: CTSO (for rat form: ab200735, Abcam, for human form: HPA002041, Sigma-Aldrich), cleaved caspase 3 (9664, Cell Signalling Technology), P-FAK (8556, Cell Signalling Technology), FAK (3285, Cell Signalling Technology), Fibronectin (15613-1-AP, Proteintech), type I collagen (14695-1-AP, Proteintech). Equal loading was checked by reprobing of the membrane with an anti-tubulin antibody (T9026, Sigma). Immune complexes were detected with appropriate secondary antibodies and enhanced chemiluminescence reagent (Clarity ECL BioRad). Protein band intensities were quantified using ImageJ Software (NIH software, Bethesda, Md)

***Ctso* silencing**

VSMC were transfected using Lipofectamine RNAiMAX reagent (Invitrogen) according to the manufacturer instructions with a pool of siRNAs targeting rat *Ctso* (ON-TARGETplus siRNA-SMARTpool (Cat# L-110260-00-0005; Horizon Discovery,) and a non-targeting control pool (Pool #1, D-001810-10-05, Horizon Discovery) to generate KD-SMC and Cont-SMC, respectively. The efficiency of *Ctso* mRNA depletion was assessed 72 h post-transfection by RT-qPCR.

Viability/Proliferation assay

VSMC viability/proliferation was quantified by MTT (3-[4,5 Dimethylthiazol-2-yl]-2,5-diphenyltetrazodium) colorimetric assay according to the manufacturer instructions (M5655; Sigma aldrich). Briefly, VSMC were seeded onto 96-well plates in triplicate for each condition, cultured for 24 h, after which they were serum-starved for 24 h. VSMC were then incubated in DMEM without or with 10% FBS for 24h. The number of viable cells was then determined by incubation in 1 mg/mL MTT for 4 h à 37 °C. The medium was then removed and acidified isopropanol was added to solubilize the MTT reduction product formazan. MTT reduction by viable cells was then quantified by measurement of the absorbance at 590 nm.

Apoptosis assay

VSMC apoptosis was determined after incubation in 1 µmol/L staurosporine (S5921, Sigma Aldrich) in serum-free medium for 8 h. Apoptosis was quantified by the measurement of cleaved caspase 3 by western blot and by TUNEL assay. VSMC were fixed with 4% paraformaldehyde and permeabilized. Fragmented DNA was stained with TUNEL Assay Kit - BrdU-Red (ab66110, Abcam) according to manufacturer instructions, and DAPI was used to label all nuclei. Coverslips were mounted on slides with Prolong gold antifade reagent and

observed with a fluorescent microscope. Apopotic cell number was quantified as the percentage of TUNEL-positive cells.

Transwell migration assay

Boyden chamber assay was performed as previously described.[47] VSMC, transfected with siRNA 48 h before, were trypsinized and washed in serum-free DMEM before plating into transwells (0.47cm^2 of culture area, 8 µm pore size; Nunc™). DMEM containing 10% FCS was placed in the lower chamber and VSMC were allowed to migrate for 10 h at 37 °C. After incubation, the filter was removed and VSMC on the upper side of the filter were scraped off. VSMC that had migrated to the lower side of the filter were fixed with 4% paraformaldehyde and stained with Coomassie blue 0.1% for observation under a microscope in brightfield mode. Migration to the lower chamber of the transwell was quantified by the area covered by cells measured using ImageJ Software and expressed expressed relative to Cont-SMC set as 1.

Cell adhesion assay using impedance technology

VSMC (10000/well) were seeded in a 96 well plate microtiter xCELLigence assay plate coated with 2 µg/ml fibronectin (E-Plate, ACEA Biosciences Inc.) and placed on the Real-time xCELLigence Cell Analyzer (Roche Applied Science) platform at 37°C. The cell index value, which are proportionate to the area covered by the cells was measured every 5 min for a period of 8 h. Adhesion speed was defined as the slope of the cell index change over time.

Collagen gel contraction assay

VSMC were mixed with collagen gel working solution (CBA-201, Cell Biolabs). The cell-collagen mixture was added into a 24-well plate and incubated at 37°C for 1 h to allow collagen polymerization. Serum-free DMEM was added to the top of the collagen gel lattice.

After 24 h, cells were treated or not with U46619 (10^{-6} mol/L) and the myosin inhibitor BDM (from CBA-201 kit), and the collagen gels were released by a sterile spatula. Changes in the collagen gel area were measured at 48 h. The percentage of contraction corresponded to [(area in BDM condition-area in the control or U46619 condition)/ area in BDM condition × 100],

Atomic force microscopy (AFM) experiments

AFM experiments have been performed in Cont- and KD-SMC grown on plastic and allowed to produce their own ECM for 5 days. ECM analysis has been performed after decellularization as previously described. All experiments were then performed in Physiological Saline Solutions (PSS) buffered with 20 mM HEPES at 37°C using a NanoWizard® atomic force microscope (JPK Instruments, Germany) equipped with a temperature controller and inverted optical microscope. Indentation experiments were carried out with cantilevers (SQube) having a colloidal glass sphere of 5 µm in diameter. Their spring constant was calibrated using the thermal noise method implemented in the AFM setting (JPK software), with values comprised between 0.12 and 0.15 $N.m^{-1}$. Prior to indentation measurements, the cantilever sensitivity was systematically measured from the slope of force-distance curves performed on glass. The optical microscope was first used to position the AFM tip on ECM or on the cytoplasmic region of the selected cell and several approach-retract force-distance curves were performed to determine the force to be applied corresponding to an indentation depth of ~500 nm (a good compromise avoiding the long-range interactions and in the validity domain of the Hertz contact mechanics model). Then, force-distance curves were recorded on cells at a low constant speed of 1 µm/s to neglect the hydrodynamic drag forces exerted on the cantilever by the liquid medium.[48] These curves were then converted into force-indentation curves, and the approach part was fitted by the Hertz model to determine the apparent elastic modulus of cells.[49]

Mutagenesis

CTSO-TurboGFPpPlasmid was purchased from Origene (RG208268). c.128C>T *CTSO* and c.946G>A *CTSO* mutagenesis was performed using Q5® Site-Directed Mutagenesis Kit Protocol (E0554, NEB) and designed primers: A43V-Fw: 5'-GAA GCCGCCGTCTTCCGGGAAAGTC-3'; A43V-Rv: 5'-ACG CTCGCGGCTCCGCGG-3'; V316I-Fw: 5'-GTTTGTGGTATTGCAGATTCCATTTCTTCTATATTTGTGACGC-3'; V316I-Rv: 5'-GCGTCACAAATATAGAAGAAATGGAATCTGCAATACCACAAAC-3'. Mutations were confirmed by standard sequencing methods using T7 standard primer and designed primer (5'-AAGCCCCTGGAAGACCTAAG-3') .

Generation of lentiviral constructs

From LT3GEPIR plasmid (#111177, Addgene), was modified to remove miR30 backbone by amplifying and cloning eGFP between XhoI and EcoRI restriction sites using the following primers: Fw 5'-CGGCCGCTCGAGATGGTGAGCAAGGGCGAGGAG-3'and Rv 5' GATCTGAATTCTTACTTGTACAGCTCGTCCATGC-3'. The resulting plasmid was used to clone WT and mutant CTSO in BamHI and XhoI,

Lentivirus production, transduction and induction of WT-CTSO and CTSO variants

Lentiviral vector for expressing WT-CTSO, p.Ala43Val-CTSO and p.Val316Ile-CTSO was transfected into HEK293T cells along with packaging vectors psPAX2 and pVSVG2 (provided by Prof. Dr.Utz Fischer's lab) using polyethylenimine (#764965, Sigma-Aldrich) transfection agent. After overnight incubation, the medium was replaced with fresh medium (DMEM+10% serum). Forty-eight hours and 72 h after transfection, viral supernatant was collected, filtered through 0.22 μm filter and used to infect NIH3T3 in the presence of

polybrene (8 µg/mL, H9268; Sigma Aldrich). After 48 to 72 h of infection, transduced NIH3T3 cells were selected with puromycin (2 µg/mL, P8833, Sigma Aldrich) for 48 h and maintained in the presence of puromycin (2 µg/mL). The induction of WT- or mutated CTSO was performed at least 2 days before the experiment by supplementing the medium with doxycycline (1 µg/mL, #D9891, Sigma Aldrich), which was maintained until the completion of the experimental procedure.

Statistical analysis

Statistical analysis was performed using GraphPad Prism software. Details of the statistical test used for each experiment is indicated in the figure legends.

Acknowledgements

We are grateful to the Genomics and Bioinformatics Core Facilities (GenoA and BiRD) and to the animal house facility (UTE) of Nantes Université for their expert services. We would like to thank the Genome Aggregation Database (gnomAD) and the groups that provided exome and genome variant data to this resource. A full list of contributing groups can be found at http://gnomad.broadinstitute.org/about. We acknowledge the Center of Biological Resources (CHU Nantes, Hoôtel-Dieu, CBR, Nantes, France) as well as Martine and Marie-France Le Cunff and the Clinical Investigation Center 1413 of Nantes for their assistance in managing the ICAN and PREGO biobanks.

Sources of Funding

This work was supported by the French national research agency (ANR) (Programme d'Investissements d'Avenir ANR-16-IDEX-0007 [NeXT Initiative], ANR-21-CE17-0006 [to RBo] and ANR-21-CE14-0016 [to A-CV]), Fondation pour la Recherche Médicale

(R22131NN - RAD22168NNA to GL), Institut de France – Académie des Sciences (Lamonica Award to GL, supporting M-AM) and the local fund Genavie (to MF and RR).

Disclosures

The authors have reported that they have no relationships with industry relevant to the contents of this paper to disclose.

Author contributions

HD and RBo supervised patient recruitment and DNA biobanking. RBo, CD and RR conceived and directed the genetic investigations. RBl, SBe, SBo, PL, FB, and JFD generated and analyzed the genetic data. MF, M-AR, and MR performed experiments in VSMC, collected the data and analyzed the results. SPRB designed the lentiviral constructs and made the mutant cells. SC performed AFM and analyzed the results. ACV designed the in vitro study, analyzed the results, and reviewed the manuscript. GL conceived and directed the in vitro study. RBo, GL, and RR supervised the work and wrote the manuscript with input from all authors. All authors reviewed the results and approved the final version of the manuscript

References

1. Vlak MH, Algra A, Brandenburg R, Rinkel GJ. Prevalence of unruptured intracranial aneurysms, with emphasis on sex, age, comorbidity, country, and time period: A systematic review and meta-analysis. *Lancet Neurol*. 2011;10:626-636
2. Nieuwkamp DJ, Setz LE, Algra A, Linn FH, de Rooij NK, Rinkel GJ. Changes in case fatality of aneurysmal subarachnoid haemorrhage over time, according to age, sex, and region: A meta-analysis. *Lancet Neurol*. 2009;8:635-642
3. Steiner T, Juvela S, Unterberg A, Jung C, Forsting M, Rinkel G, et al. European stroke organization guidelines for the management of intracranial aneurysms and subarachnoid haemorrhage. *Cerebrovasc Dis*. 2013;35:93-112
4. Vlak MH, Rinkel GJ, Greebe P, Algra A. Risk of rupture of an intracranial aneurysm based on patient characteristics: A case-control study. *Stroke*. 2013;44:1256-1259
5. Bourcier R, Redon R, Desal H. Genetic investigations on intracranial aneurysm: Update and perspectives. *J Neuroradiology*. 2015;42:67-71
6. Kissela BM, Sauerbeck L, Woo D, Khoury J, Carrozzella J, Pancioli A, et al. Subarachnoid hemorrhage - a preventable disease with a heritable component. *Stroke*. 2002;33:1321-1326
7. Bilguvar K, Yasuno K, Niemela M, Ruigrok YM, von Und Zu Fraunberg M, van Duijn CM, et al. Susceptibility loci for intracranial aneurysm in european and japanese populations. *Nat Genet*. 2008;40:1472-1477
8. Yasuno K, Bakircioglu M, Low SK, Bilguvar K, Gaal E, Ruigrok YM, et al. Common variant near the endothelin receptor type a (ednra) gene is associated with intracranial aneurysm risk. *Proc Natl Acad Sci U S A*. 2011;108:19707-19712
9. Yasuno K, Bilguvar K, Bijlenga P, Low SK, Krischek B, Auburger G, et al. Genome-wide association study of intracranial aneurysm identifies three new risk loci. *Nat Genet*. 2010;42:420-425
10. Bakker MK, van der Spek RAA, van Rheenen W, Morel S, Bourcier R, Hostettler IC, et al. Genome-wide association study of intracranial aneurysms identifies 17 risk loci and genetic overlap with clinical risk factors. *Nat Genet*. 2020;52:1303-1313
11. Zhou S, Ambalavanan A, Rochefort D, Xie P, Bourassa CV, Hince P, et al. Rnf213 is associated with intracranial aneurysms in the french-canadian population. *Am J Hum Genet*. 2016;99:1072-1085
12. Santiago-Sim T, Fang X, Hennessy ML, Nalbach SV, DePalma SR, Lee MS, et al. Thsd1 (thrombospondin type 1 domain containing protein 1) mutation in the pathogenesis of intracranial aneurysm and subarachnoid hemorrhage. *Stroke*. 2016;47:3005-3013
13. Wu YQ, Li ZL, Shi Y, Chen LY, Tan HB, Wang ZY, et al. Exome sequencing identifies loxl2 mutation as a cause of familial intracranial aneurysm. *World Neurosurgery*. 2018;109:E812-E818
14. Lorenzo-Betancor O, Blackburn PR, Edwards E, Vazquez-do-Campo R, Klee EW, Labbe C, et al. Pcnt point mutations and familial intracranial aneurysms. *Neurology*. 2018;91:E2170-E2181
15. Yang X, Li J, Fang Y, Zhang Z, Jin D, Chen X, et al. Rho guanine nucleotide exchange factor arhgef17 is a risk gene for intracranial aneurysms. *Circ Genom Precis Med*. 2018;11:e002099
16. Bourcier R, Le Scouarnec S, Bonnaud S, Karakachoff M, Bourcereau E, Heurtebise-Chretien S, et al. Rare coding variants in angptl6 are associated with familial forms of intracranial aneurysm. *Am J Hum Genet*. 2018;102:133-141
17. Barak T, Ristori E, Ercan-Sencicek AG, Miyagishima DF, Nelson-Williams C, Dong W, et al. Ppil4 is essential for brain angiogenesis and implicated in intracranial aneurysms in humans. *Nat Med*. 2021;27:2165-2175
18. Reiser J, Adair B, Reinheckel T. Specialized roles for cysteine cathepsins in health and disease. *J Clin Invest*. 2010;120:3421-3431

19. Hedin U, Bottger BA, Forsberg E, Johansson S, Thyberg J. Diverse effects of fibronectin and laminin on phenotypic properties of cultured arterial smooth muscle cells. *J Cell Biol*. 1988;107:307-319
20. Yang P, Troncone L, Augur ZM, Kim SSJ, McNeil ME, Yu PB. The role of bone morphogenetic protein signaling in vascular calcification. *Bone*. 2020;141:115542
21. Matsukawa H, Shinoda M, Fujii M, Uemura A, Takahashi O, Niimi Y. Arterial stiffness as a risk factor for cerebral aneurysm. *Acta Neurol Scand*. 2014;130:394-399
22. Vlak MH, Rinkel GJ, Greebe P, Algra A. Independent risk factors for intracranial aneurysms and their joint effect: A case-control study. *Stroke*. 2013;44:984-987
23. Hudson JS, Hoyne DS, Hasan DM. Inflammation and human cerebral aneurysms: Current and future treatment prospects. *Future Neurol*. 2013;8
24. Ketscher A, Ketterer S, Dollwet-Mack S, Reif U, Reinheckel T. Neuroectoderm-specific deletion of cathepsin d in mice models human inherited neuronal ceroid lipofuscinosis type 10. *Biochimie*. 2016;122:219-226
25. Vidak E, Javorsek U, Vizovisek M, Turk B. Cysteine cathepsins and their extracellular roles: Shaping the microenvironment. *Cells*. 2019;8
26. Yadati T, Houben T, Bitorina A, Shiri-Sverdlov R. The ins and outs of cathepsins: Physiological function and role in disease management. *Cells*. 2020;9
27. Wu H, Du Q, Dai Q, Ge J, Cheng X. Cysteine protease cathepsins in atherosclerotic cardiovascular diseases. *J Atheroscler Thromb*. 2018;25:111-123
28. Liu CL, Guo J, Zhang X, Sukhova GK, Libby P, Shi GP. Cysteine protease cathepsins in cardiovascular disease: From basic research to clinical trials. *Nat Rev Cardiol*. 2018;15:351-370
29. Aoki T, Kataoka H, Ishibashi R, Nozaki K, Hashimoto N. Cathepsin b, k, and s are expressed in cerebral aneurysms and promote the progression of cerebral aneurysms. *Stroke*. 2008;39:2603-2610
30. Lacolley P, Regnault V, Avolio AP. Smooth muscle cell and arterial aging: Basic and clinical aspects. *Cardiovasc Res*. 2018;114:513-528
31. Saphirstein RJ, Gao YZ, Jensen MH, Gallant CM, Vetterkind S, Moore JR, et al. The focal adhesion: A regulated component of aortic stiffness. *PLoS One*. 2013;8:e62461
32. Sehgel NL, Sun Z, Hong Z, Hunter WC, Hill MA, Vatner DE, et al. Augmented vascular smooth muscle cell stiffness and adhesion when hypertension is superimposed on aging. *Hypertension*. 2015;65:370-377
33. Lobert VH, Brech A, Pedersen NM, Wesche J, Oppelt A, Malerod L, et al. Ubiquitination of alpha 5 beta 1 integrin controls fibroblast migration through lysosomal degradation of fibronectin-integrin complexes. *Dev Cell*. 2010;19:148-159
34. Buck MR, Karustis DG, Day NA, Honn KV, Sloane BF. Degradation of extracellular-matrix proteins by human cathepsin b from normal and tumour tissues. *Biochem J*. 1992;282 (Pt 1):273-278
35. Nettesheim A, Shim MS, Dixon A, Raychaudhuri U, Gong H, Liton PB. Cathepsin b localizes in the caveolae and participates in the proteolytic cascade in trabecular meshwork cells. Potential new drug target for the treatment of glaucoma. *J Clin Med*. 2020;10
36. Qiu H, Zhu Y, Sun Z, Trzeciakowski JP, Gansner M, Depre C, et al. Short communication: Vascular smooth muscle cell stiffness as a mechanism for increased aortic stiffness with aging. *Circ Res*. 2010;107:615-619
37. Wheeler JB, Mukherjee R, Stroud RE, Jones JA, Ikonomidis JS. Relation of murine thoracic aortic structural and cellular changes with aging to passive and active mechanical properties. *J Am Heart Assoc*. 2015;4:e001744
38. Nolasco P, Fernandes CG, Ribeiro-Silva JC, Oliveira PVS, Sacrini M, de Brito IV, et al. Impaired vascular smooth muscle cell force-generating capacity and phenotypic deregulation in marfan syndrome mice. *Biochim Biophys Acta Mol Basis Dis*. 2020;1866:165587

39. Crosas-Molist E, Meirelles T, Lopez-Luque J, Serra-Peinado C, Selva J, Caja L, et al. Vascular smooth muscle cell phenotypic changes in patients with marfan syndrome. *Arterioscler Thromb Vasc Biol*. 2015;35:960-972
40. Kim JH, Kim JW, Song SW, Ahn SJ, Park M, Park SK, et al. Intracranial aneurysms are associated with marfan syndrome: Single cohort retrospective study in 118 patients using brain imaging. *Stroke*. 2021;52:331-334
41. Bourcier R, Chatel S, Bourcereau E, Jouan S, Marec HL, Daumas-Duport B, et al. Understanding the pathophysiology of intracranial aneurysm: The ican project. *Neurosurgery*. 2017;80:621-626
42. Li H, Durbin R. Fast and accurate long-read alignment with burrows-wheeler transform. *Bioinformatics*. 2010;26:589-595
43. Poplin R, Ruano-Rubio V, DePristo MA, Fennell TJ, Carneiro MO, Van der Auwera GA, et al. Scaling accurate genetic variant discovery to tens of thousands of samples. *bioRxiv*. 2018:201178
44. Karczewski KJ, Solomonson M, Chao KR, Goodrich JK, Tiao G, Lu W, et al. Systematic single-variant and gene-based association testing of thousands of phenotypes in 394,841 uk biobank exomes. *Cell Genomics*. 2022;2:100168
45. Alves I, Giemza J, Blum M, Bernhardsson C, Chatel S, Karakachoff M, et al. Genetic population structure across brittany and the downstream loire basin provides new insights on the demographic history of western europe. *bioRxiv*. 2022:2022.2002.2003.478491
46. Han L, Abney M. Identity by descent estimation with dense genome-wide genotype data. *Genet Epidemiol*. 2011;35:557-567
47. Goueffic Y, Guilluy C, Guerin P, Patra P, Pacaud P, Loirand G. Hyaluronan induces vascular smooth muscle cell migration through rhamm-mediated pi3k-dependent rac activation. *Cardiovasc Res*. 2006;72:339-348
48. Cuenot S, Gelebart P, Sinquin C, Colliec-Jouault S, Zykwinska A. Mechanical relaxations of hydrogels governed by their physical or chemical crosslinks. *J Mech Behav Biomed Mater*. 2022;133:105343
49. Zykwinska A, Makshakova O, Gelebart P, Sinquin C, Stephant N, Colliec-Jouault S, et al. Interactions between infernan and calcium: From the molecular level to the mechanical properties of microgels. *Carbohydr Polym*. 2022;292:119629

Figures Legends

Figure 1 Pedigree of large family with IA used for genetic investigations

A Pedigree of family A showing phenotypic and genetic segregation patterns. WE sequenced and genotyped individuals are respectively indicated with a red circle and a green discontinuous trait. Bold arrow indicates index case. Presence or absence of *CTSO* c.946G>A variant was assessed through capillary sequencing. **B** Pedigree for family B showing phenotypic and genetic segregation patterns. WE sequenced individual is indicated with a red circle. Bold arrow indicates index case. Presence or absence of *CTSO* c.128C>T variant was assessed through capillary sequencing.

Figure 2 Expression of CTSO and consequence of CTSO depletion on VSMC proliferation and apoptosis

A *Ctso* mRNA expression analyzed by quantitative RT-PCR in cerebral arteries of normotensive (WKY), and hypertensive rats (SHR and SHRSP). **B** *Ctso* mRNA expression analyzed by quantitative RT-PCR in VSMC cultured in static condition and subjected to 10% and 20% cyclic stretch. **C** Representative western blots and quantification of CTSO protein expression assessed in cell lysate and culture medium of VSMC cultured in static condition and subjected to 10% and 20% cyclic stretch. **D** Proliferation assessed by the measurement of MTT absorbance in the absence and presence of 10 % serum in VSMC transfected with siRNA targeting *Ctso* (KD-SMC) and control siRNA (Cont-SMC). **E** Number of apoptic cells in KD-SMC and Cont-SMC culture after stimulation with staurospaurine (1 µmol/L, 8 h). Values represent the percentage of TUNEL-positive cells relative to total cell population in each group. **F** Typical Western blot of cleaved-caspase 3 in Cont- and KD-SMC and corresponding quantification. CTSO and tubulin have been also blotted to check CTSO

silencing and equal loading. Results are expressed relative to Cont-SMC set as 1. (Data are expressed as mean ± SEM; *p<0.05; **p<0.01 and ***p<0.01; one-way *ANOVA*)

Figure 3 CTSO depletion in VSMC decreases migration, stimulates adhesion, FAK phosphorylation and FN expression

A Representative images of Cont- and KD-SMC which migrated to the underside surface of Transwell membranes and the corresponding quantification. **B** Representative curve showing the cell index representing the adhesion of Cont- and KD-SMC over time and quantification of the adhesion speed. **C** and **D** Representative Western blots showing the phosphorylation of FAK in Cont- and KD-SMC 2 h and 24 h after seeding on FN matrix (C) or directly on plastic (D). Graphs show densitometric analysis of phospho-FAK in blots, relative to FAK expression. **E** Representative western blots showing the amount of FN and Col-I in Cont- and KD-SMC and corresponding quantification. (Results were expressed relative to Cont-SMC and presented as mean ± SEM; *p < 0.05, *p < 0.01; Mann-Whitney test).

Figure 4 CTSO depletion in VSMC modulates contractile phenotype marker expression, contraction and cell stifnesss

A-C RT-qPCR analysis of mRNA levels of Col1A, Fn1 (A); of the SMC marker gene *Acta2*, *Myh11*, *Talgn*, *Cnn1* (B); and *Bmp4* and *Ctso* (C) in Cont- and KD-SMC. Results were expressed relative to Cont-SMC. **D** Representative images of Cont-SMC- and KD-SMC-seeded collagen gels 48 h after release with and without U46619 and quantification of U46619-induced gel contraction in Cont- and KD-SMC. **E** Atomic force microscopy determination of the elastic modulus of Cont- and KD-SMC (left) and their respective extracellular matrix (right). (Data are expressed as mean ± SEM; *p < 0.05, *p < 0.01; Mann-Whitney test).

Figure 5 CTSO variants weakly secreted and induced increase in FN

A Representative western blots and quantification of CTSO protein expression measured in cell lysate and culture medium of NIH3T3 expressing WT-CTSO, p.Ala43Val-CTSO and p.Val316Ile-CTSO. **B** Representative western blots and quantification of FN and Col-1 expression measured in WT-CTSO, p.Ala43Val-CTSO and p.Val316Ile-CTSO. (Data are expressed as mean ± SEM; *p<0.05 and ***p<0.01; one-way *ANOVA*)

Tables

Table 1 Genetic finding by whole-exome sequencing in family A

	II:9	III:4	III:2
Total variants	19583	20220	20081
Functional variants	6378	6566	6417
MAF <0.1% (GnomAD NFE)	177	179	153
Shared by the 3 relatives	16		
Shared by all affected (IBD)	1 (CTSO)		

Table 2 Rare coding variants found across families A and B in *CTSO*.

Family	Genomic position (GRCh37/hg19)	Gene	Nucleotide consequence	Protein consequence	MAF (NFE in gnomAD)	Predicted Functional Impact		Cases / Total	
						SIFT	Polyphen 2	Affected	Unaffected
A	4:156847208	*CTSO*	c.946G>A	p.Val316Ile	$1.7.10^{-5}$	Deleterious	Probably damaging	6/6	6/17
B	4:156874872	*CTSO*	c.128C>T	p.Ala43Val	$3.0.10^{-4}$	Tolerated	Probably damaging	3/3	0/5

Mutation names are based on Ensembl *CTSO* transcript ENST00000433477.3. MAF: Minor Allele Frequency; NFE: Exome Aggregation Consortium (Non-Finnish Europeans); gnomAD: Genome Aggregation Database; GERP: Genomic Evolutionary Rate Profiling; SIFT: Sorting Intolerant From Tolerant.

Table 3 Clinical characteristics, treatments and exposition to risk factors for IA cases and unaffected relatives according to *CTSO* status.

	***CTSO* variants IA**	***CTSO* variants no IA**	**No *CTSO* variant no IA**	***P*-value**
n	11	6	18	-
Female	8 (72.73%)	2 (33.33%)	10 (55.56%)	0.32
Age	63.00 (56.00 - 75.50)	63.50 (60.25 - 81.00)	46.50 (38.50 - 53.75)	0.53
Smoker or former Smoker	6 (54.55%)	4 (66.67%)	9 (50.00%)	0.90
Alcohol intake per week > 150g	5 (45.45%)	1 (16.67%)	3 (16.67%)	0.23
High Blood Pressure	**5 (45.45%)**	**2 (33.33%)**	**1 (5.56%)**	**0.023**
Dyslipemia or diabetes	2 (18.18%)	1 (16.67%)	1 (5.56%)	0.47
Antiplatelet treatment	3 (27.27%)	1 (16.67%)	1 (5.56%)	0.22
Anti-inflammatory Drugs	0 (0.00%)	0 (0.00%)	1 (5.56%)	1.0
Statin treatment	2 (18.18%)	1 (16.67%)	1 (5.56%)	0.47
Oral anticoagulant treatment	1 (9.09%)	2 (33.33%)	4 (22.22%)	0.55

Data are expressed as median, (minimum, and maximum) for age and as count (and percentage) for all other categorical variables. Usual bivariate parametric ($\chi 2$ test or Fisher exact test) statistical tests were used for comparison between groups.

Appendices

Consortia

The ICAN Study Group includes the following investigators: Hubert Desal, Romain Bourcier, Benjamin Daumas-Duport, Bertrand Isidor, Jérôme Connault, Pierre Lebranchu, Thierry Le Tourneau, Marie Pierre Viarouge, Chrisanthi Papagiannaki, Michel Piotin, Hocine Redjem, Mikael Mazighi, Jean Philippe Desilles, Olivier Naggara, Christine Rodriguez, Waghi Ben Hassen, Suzanna Saleme, Charbel Mounayer, Olivier Levrier, Pierre Aguettaz, Xavier Combaz, Anne Pasco, Emeline Berthier, Marc Bintner, Marc Molho, Pascale Gauthier, Cyril Chivot, Vincent Costalat, Cyril Darganzil, Alain Bonafé, Anne Christine Januel, Caterina Michelozzi, Christophe Cognard, Fabrice Bonneville, Philippe Tall, Jean Darcourt, Alessandra Biondi, Cristina Iosif, Elisa Pomero, Jean Chistophe Ferre, Jean Yves Gauvrit, François Eugene, Hélène Raoult, Jean Christophe Gentric, Julien Ognard, René Anxionnat, Serge Bracard, Anne Laure Derelle, Romain Tonnelet, Laurent Spelle, Léon Ikka, Aymeric Rouchaud, Augustin Ozanne, Gildaz Caroff, Nidal Ben Achour, Jacques Moret, Emmanuel Chabert, Jérôme Berge, Guillaume Marnat, Xavier Barreau, Florent Gariel, Frédéric Clarencon, Mohammed Aggour, Frédéric Ricolfi, Adrien Chavent, Pierre Thoant, Brivael Lemogne, Denis Herbreteau, Richard Bibi, Anna Paula Narata, Pedro Lebedenski, Laurent Pierot, Sébastien Soize, Marc Antoine Labeyrie, Christophe Vandendries, Emmanuel Houdart, Appoline Kazemi, Xavier Leclerc, Jean Pierre Pruvo, Sophie Gallas, Stéphane Velasco.

Supplemental Materials

Figure S1 and S2

Table S1 and S2

Figures

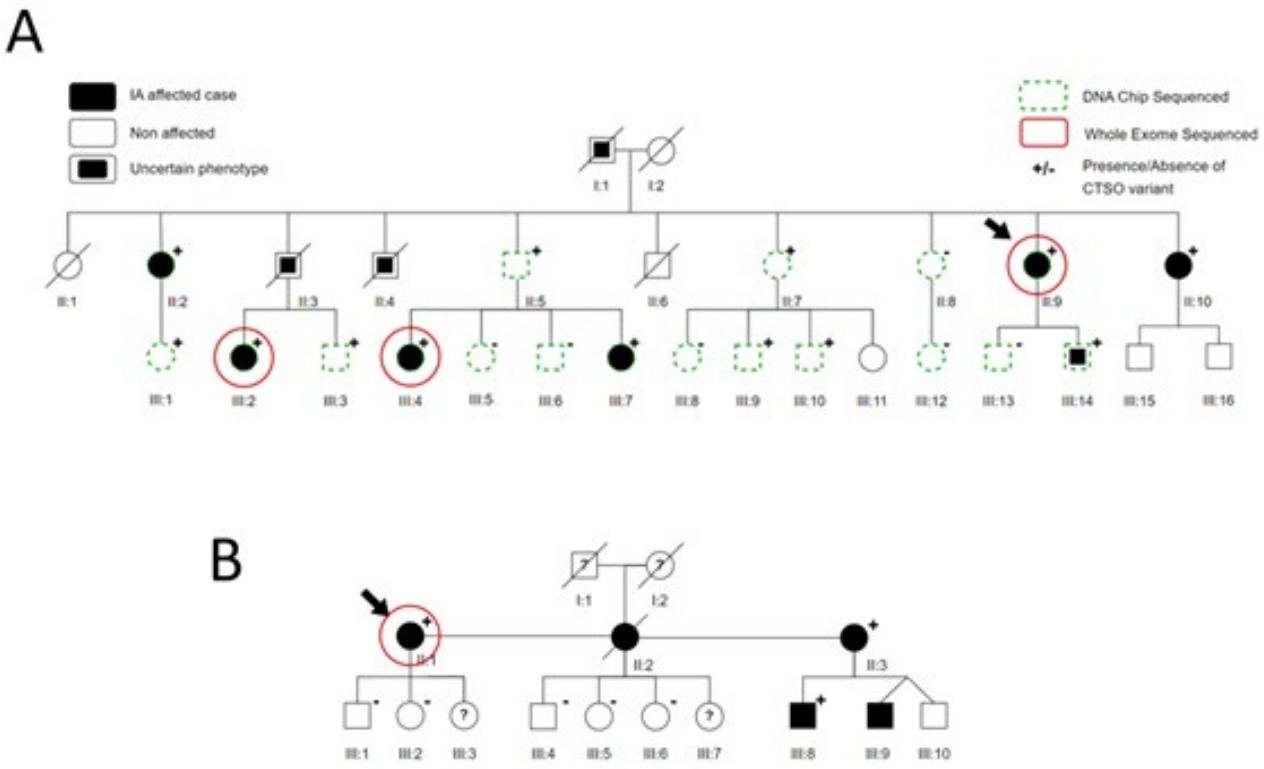

Figure 1

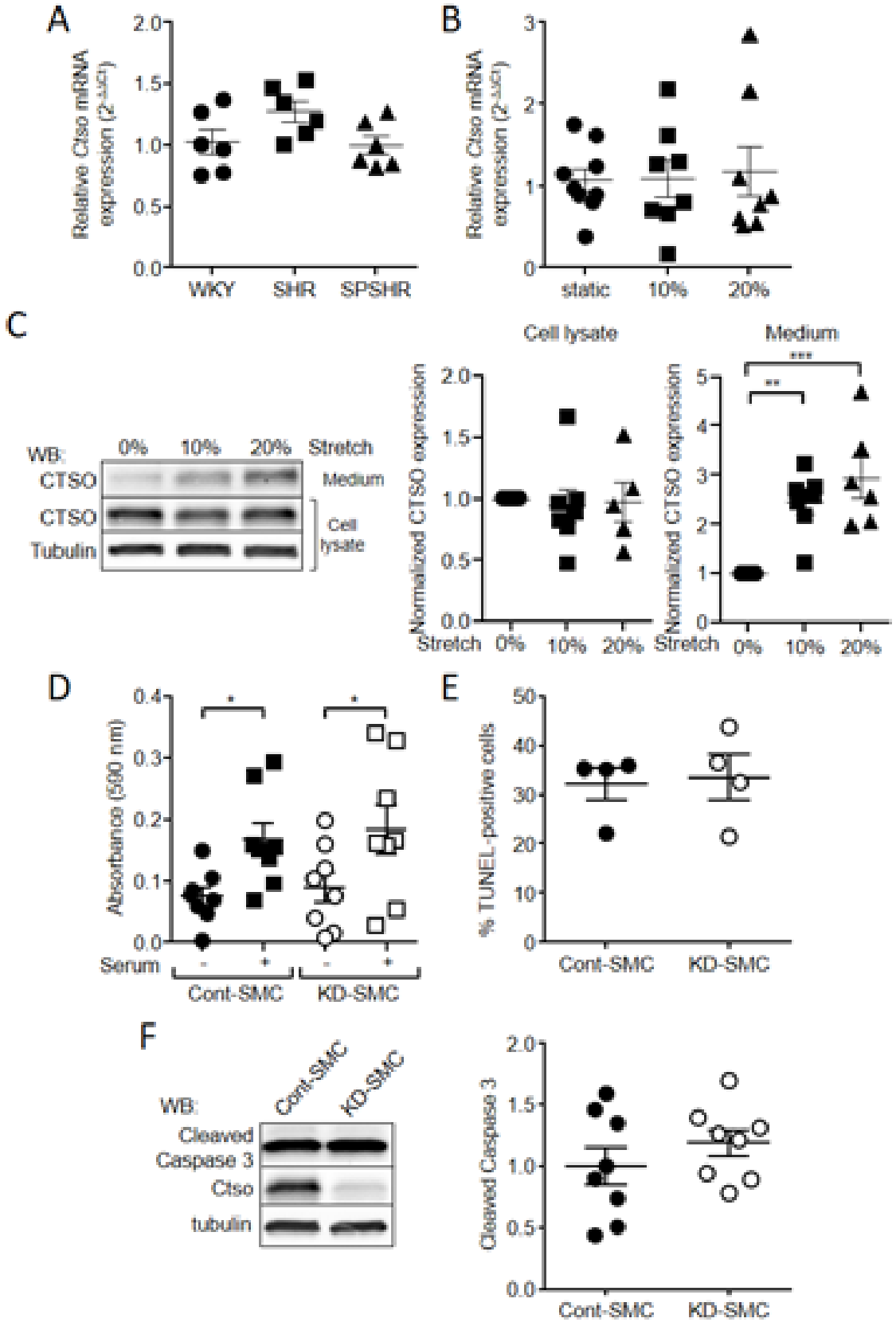
A
Relative Ctso mRNA expression ($2^{-\Delta Ct}$)
2.0
1.5
1.0
0.5
0.0
WKY
SHR
SPSHR
B
Relative Ctso mRNA expression ($2^{-\Delta Ct}$)
3
2
1
0
static
10%
20%
C
WB:
0%
10%
20%
Stretch
CTSO
Medium
CTSO
Tubulin
Cell lysate
Cell lysate
Medium
Normalized CTSO expression
2.0
1.5
1.0
0.5
0.0
Stretch 0%
10%
20%
Normalized CTSO expression
5
4
3
2
1
0
**
***
Stretch 0%
10%
20%
D
Absorbance (580 nm)
0.4
0.3
0.2
0.1
0.0
*
*
Serum
-
+
-
+
Cont-SMC
KD-SMC
E
% TUNEL-positive cells
50
40
30
20
10
0
Cont-SMC
KD-SMC
F
WB:
Cont-SMC
KD-SMC
Cleaved
Caspase 3
Ctso
tubulin
Cleaved Caspase 3
2.0
1.5
1.0
0.5
0.0
Cont-SMC
KD-SMC

Figure 2

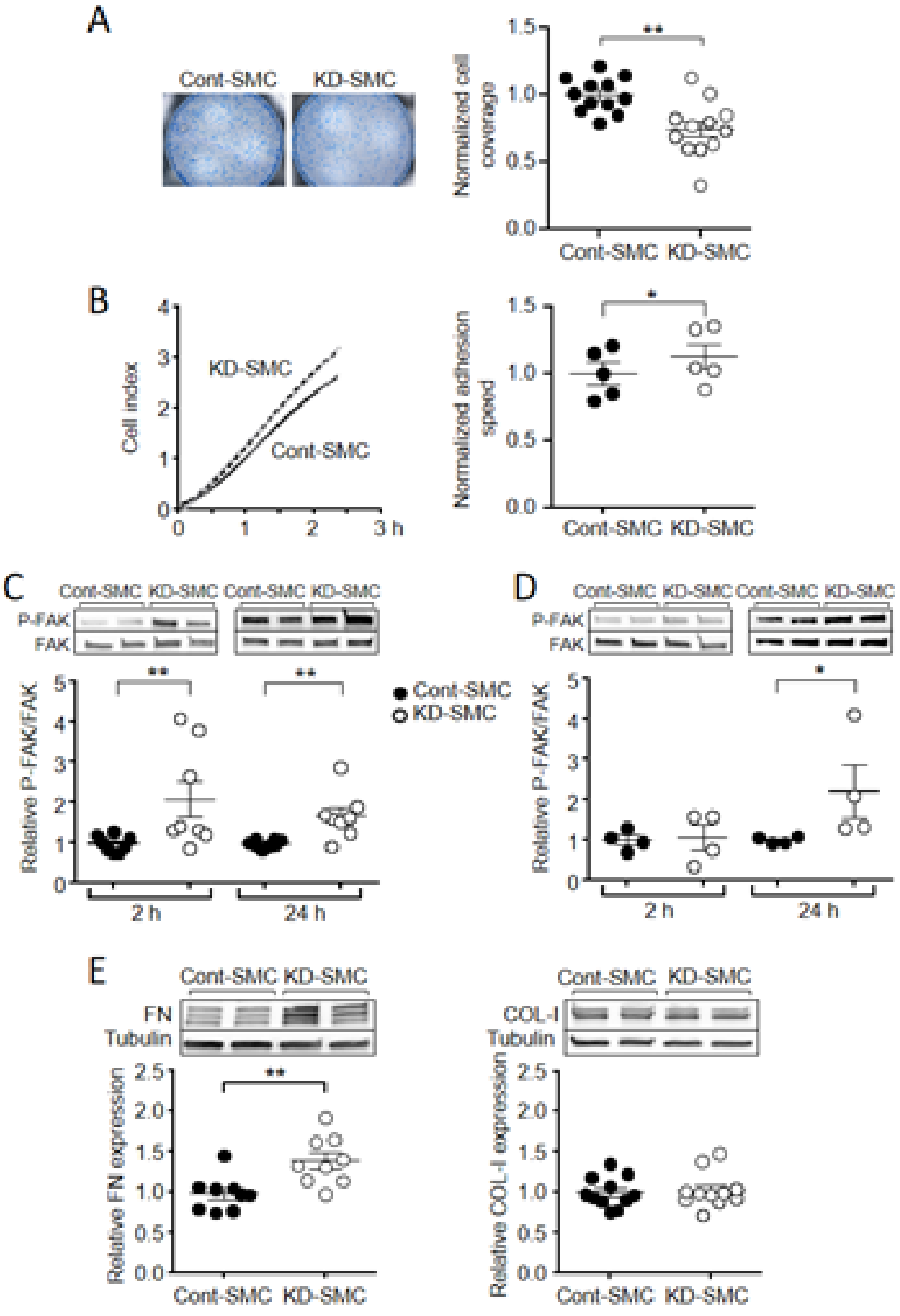
A
Cont-SMC
KD-SMC
Normalized cell coverage
1.5
1.0
0.5
0.0
**
Cont-SMC KD-SMC
B
Cell index
4
3
2
1
0
KD-SMC
Cont-SMC
0 1 2 3 h
Normalized adhesion speed
1.5
1.0
0.5
0.0
*
Cont-SMC KD-SMC
C
Cont-SMC KD-SMC Cont-SMC KD-SMC
P-FAK
FAK
Relative P-FAK/FAK
5
4
3
2
1
0
**
**
Cont-SMC
KD-SMC
2 h
24 h
D
Cont-SMC KD-SMC Cont-SMC KD-SMC
P-FAK
FAK
Relative P-FAK/FAK
5
4
3
2
1
0
*
2 h
24 h
E
Cont-SMC KD-SMC
FN
Tubulin
Relative FN expression
2.5
2.0
1.5
1.0
0.5
0.0
**
Cont-SMC KD-SMC
Cont-SMC KD-SMC
COL-I
Tubulin
Relative COL-I expression
2.5
2.0
1.5
1.0
0.5
0.0
Cont-SMC KD-SMC

Figure 3

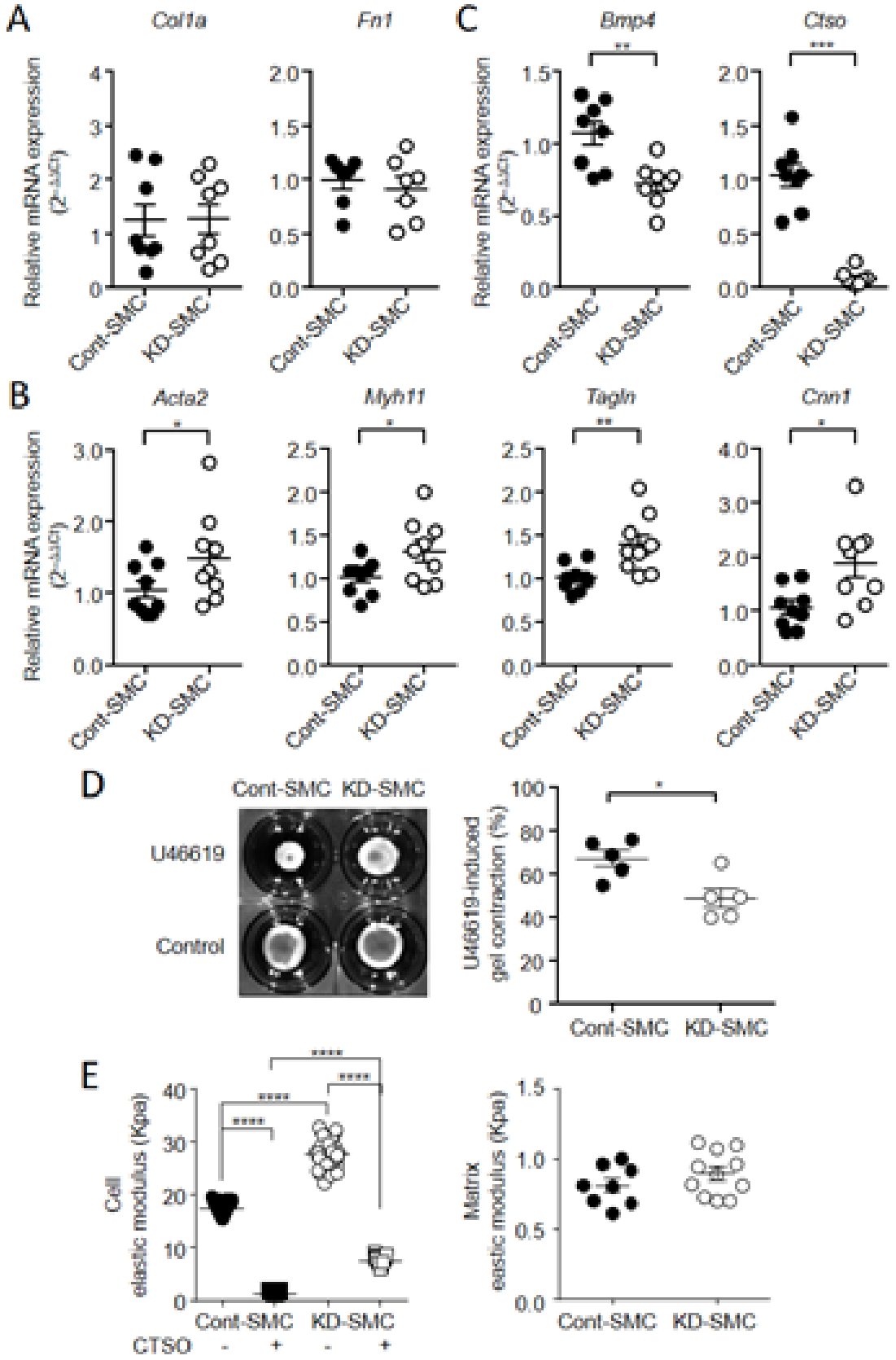
A
Col1a
Fn1
C
Bmp4
Ctso
Relative mRNA expression
Cont-SMC
KD-SMC
B
Acta2
Myh11
Tagln
Cnn1
D
Cont-SMC KD-SMC
U46619
Control
U46619-induced gel contraction (%)
E
Cell elastic modulus (Kpa)
CTSO
Matrix easic modulus (Kpa)

Figure 4

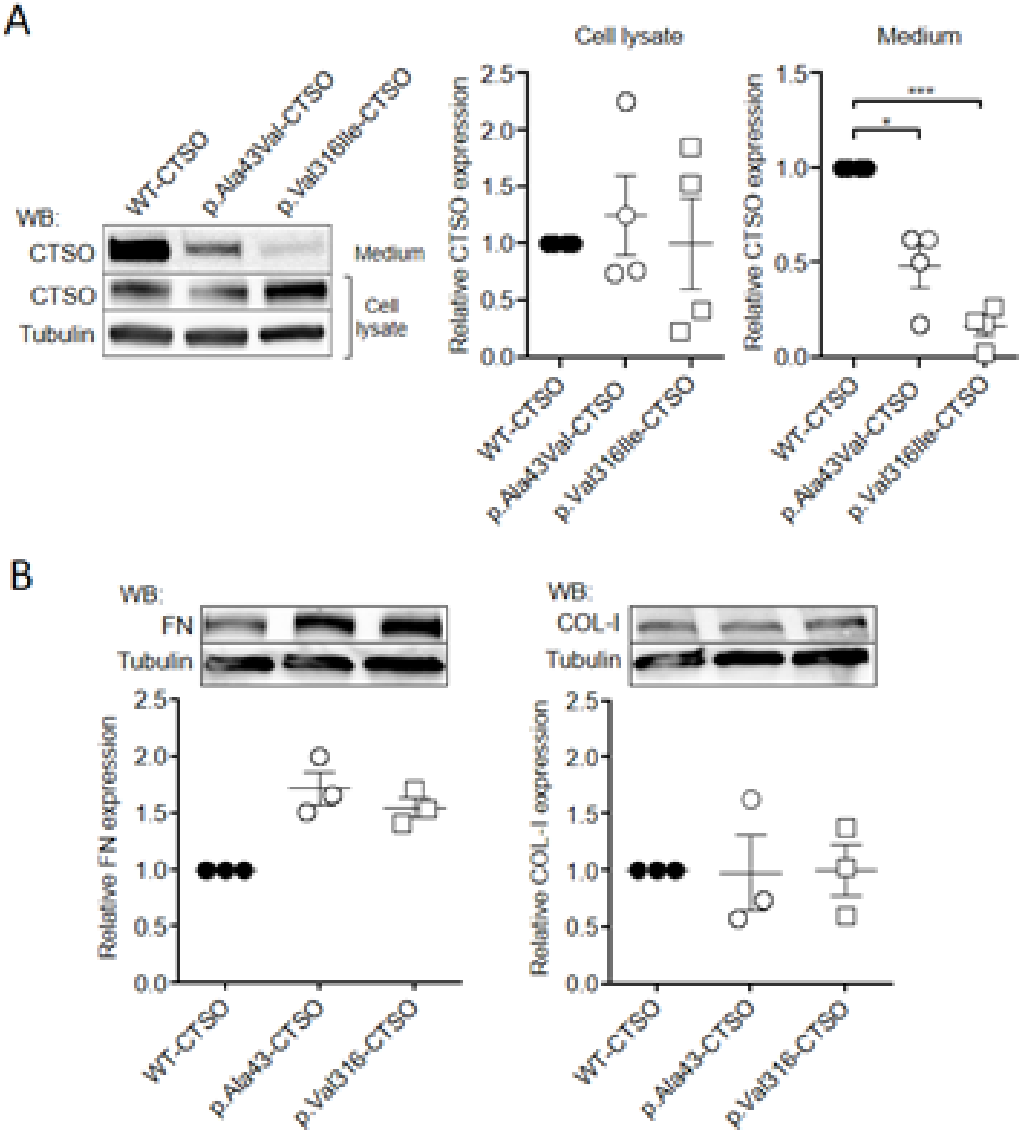
A
WT-CTSO
p.Ala43Val-CTSO
p.Val316Ile-CTSO
WB:
CTSO
CTSO
Tubulin
Medium
Cell lysate
Cell lysate
Medium
Relative CTSO expression
Relative CTSO expression
WT-CTSO
p.Ala43Val-CTSO
p.Val316Ile-CTSO
B
WB:
FN
Tubulin
WB:
COL-I
Tubulin
Relative FN expression
Relative COL-I expression
WT-CTSO
p.Ala43-CTSO
p.Val316-CTSO

Figure 5

Supplemental materials

Rare coding variants in *CTSO*, a potential new actor of arterial remodeling, are associated to familial intracranial aneurysm

Milène Freneau[1,5], Raphael Blanchet[1,5], Sandro Benichi[1], Mary-Adel Mrad[1], Surya Prakash Rao Batta[1], Marc Rio[1], Stéphanie Bonnaud[1], Pierre Lindenbaum[1], Fabien Laporte[1], Stéphane Cuénot[2], Jean-François Deleuze[3], Christian Dina[1], Stéphanie Chatel[1], Emmanuelle Bourcereau[4], Solène Jouan[4], ICAN Study Group, Hubert Desal[1,4], Anne-Clémence Vion[1], Romain Bourcier[1,4,5], Gervaise Loirand[1,5], Richard Redon[1,5].

Table S1 and S2

Figure S1 and S2

Supplemental tables

Filtering Step	Flagged Variants			Threshold
Individuals	**II:9**	**III:4**	**III:2**	
Raw data	38939	45611	44131	
Depth	6744	12803	11380	>20X
MQRS	10432	13988	13363	∈[-2.5,2.5]
MQ	5270	6563	6224	>59
Mappability	4819	6340	6135	=1
SOR	2938	3519	3389	<3
GQ	902	1156	1273	>90
LCR	787	1214	1216	
QD	366	460	444	>2
FS	113	146	168	<60
GR	7	10	5	>0.95

Table S1 Quality filtering of variants found across WES data in individuals II:9, III:2 and III:4. Abbreviations: MQRS – mapping quality rank sum; MQ – mapping quality; SOR – strand odd ratio; GQ – genotyping quality; LCR – low complexity regions; QD – quality by depth; FS – Fisher strand; GR – Genotyping Rate

Target gene	Forward primer (5'-3' sequence)	Reverse primer (5'-3' sequence)
Gapdh	AACCCATCACCATCTTCCAG	CCAGTAGACTCCACGACATAC
Ctso	CCAGATACCCAGCAAAAGGA'	ATCGCACCGCTGACTCTACT
Acta2	ACGCGAAGCTCGTTATAGAAG	GACCCTGAAGTATCCGATAGAAC
Cnn1	GATCCACTCTCTCAGCTCCT	CTTCCGCACACTTTAACCGA
Myh11	CTTTCCAGCTCCAGACTCAC	CGCCTCACATCTATGCCATT
Tagln	GCTCCTCATCATACTTCTTCTCA	AACGCTACTCTCCTTCCAG
Bmp4	ATAAAACGACCATCAGCATTCG	GCCTTTCCAGCAAGTTTGTTC'
Fn1	CGAGGTGACAGAGACCACAA	CTGGAGTCAAGCCAGACACA
Col1a	TACAGCACGCTTGTGGATGG	CAGATTGGGATGGAGGGAGTT

Table S2 Sequence of qRT-PCR primers

Supplemental Figures

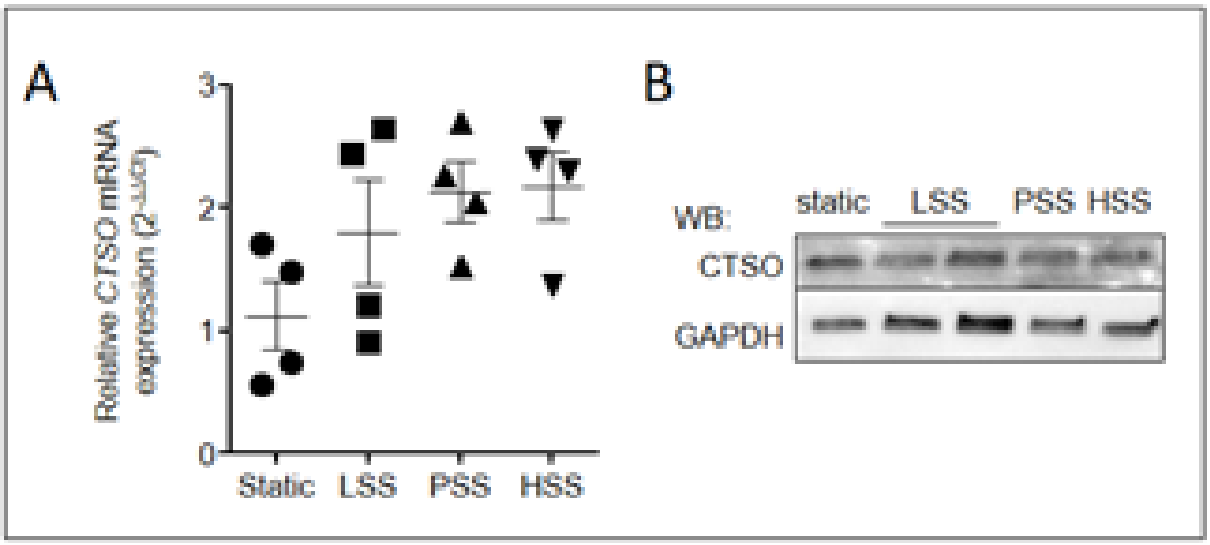

Figure S1 *CTSO* mRNA and protein expression in endothelial cells

CTSO mRNA expression analyzed by quantitative RT-PCR in HUVEC under static condition and under flow generating low (LSS, 3 dyn/cm^2), physiological (PSS, 16 dyn/cm^2) and very high (HSS, 36 dyn/cm^2) shear stress. Means ± SEM are shown. **B** Representative Western blots showing the expression of CTSO in HUVEC under static condition and under flow (LSS, PSS and HSS). Tubulin was also blotted to check equal loading.

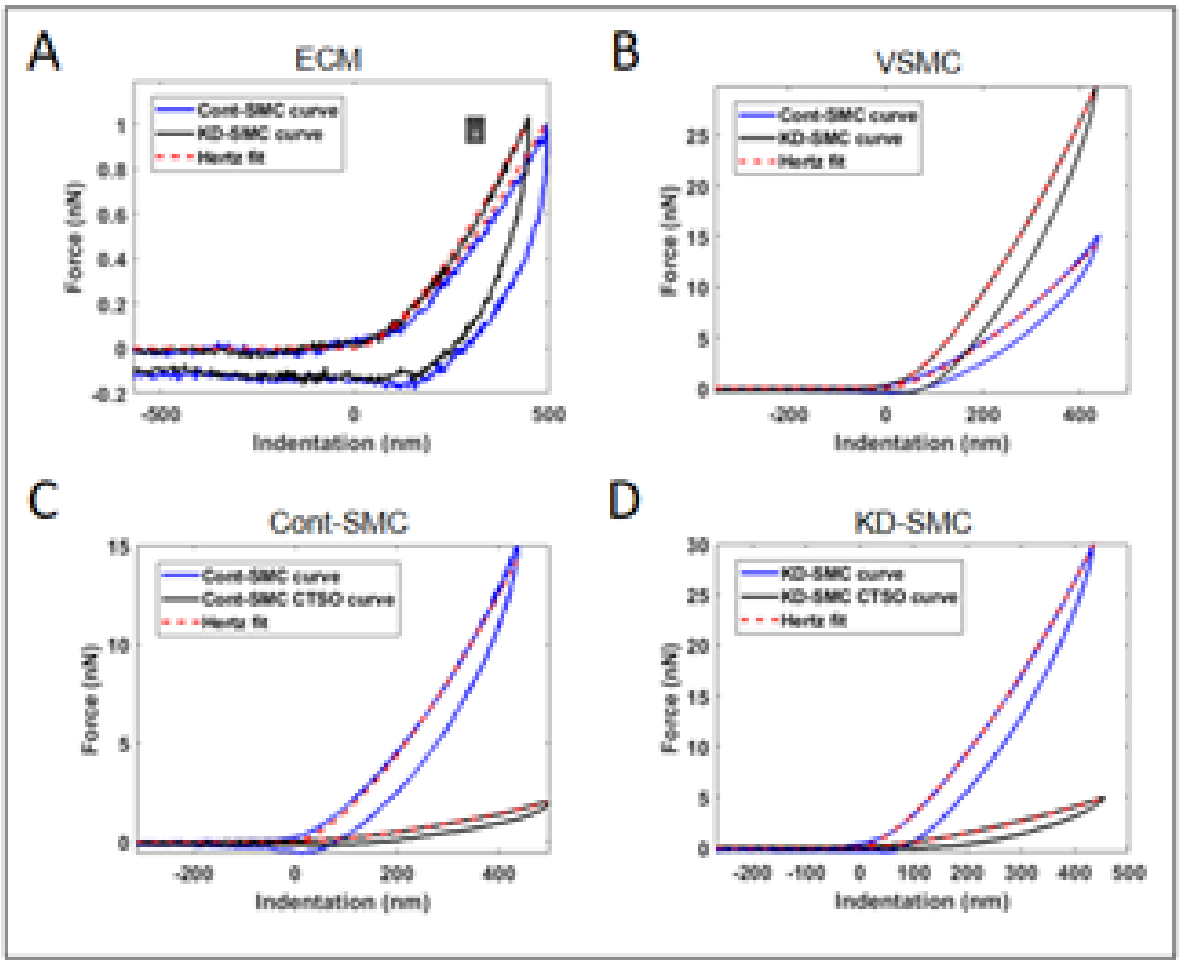

Figure S2 Analysis of VSMC and ECM by atomic force microscopy

A Representative force-indentation curves of decellularized ECM produced by Cont-SMC (blue) and KD-SMC (black). **B** Representative experimental approach-retract force-indentation curves performed on the cytoplasmic region of Cont-SMC (blue) and KD-SMC (black). **C** and **D** Representative experimental approach-retract force-indentation curves performed on the cytoplasmic region of Cont-SMC (**C**) and KD-SMC (**D**) in the absence (blue) and in the presence (black) of CTSO (200 ng/mL added 24 h prior to AFM experiments). The red curves correspond to the Hertz model fit of the approach curve to determine the apparent elastic modulus.